

Wall-pressure-array measurements beneath a separating/reattaching flow region

Laura M. Hudy and Ahmed M. Naguib^{a)}

Department of Mechanical Engineering, Michigan State University, East Lansing, Michigan 48824

William M. Humphreys, Jr.

Advanced Measurement and Diagnostics Branch, NASA Langley Research Center, Hampton, Virginia 23681

(Received 29 May 2002; accepted 5 December 2002; published 30 January 2003)

A database of wall-pressure-array measurements was compiled for studying the space–time character of the surface-pressure field within a separating/reattaching flow region. The experimental setup consisted of a long splitter plate located within the wake of a fence and instrumented with an array of flush-mounted microphones. Data were acquired for a Reynolds number of 7900, based on the fence height above the splitter plate. Two distinctive regions, defined based on their location relative to the position of the mean reattachment point (x_r) of the shear layer, emerged from this investigation. Upstream, from the fence to $0.25x_r$, the surface-pressure signature was dominated by large time scale disturbances and an upstream convection velocity of $0.21U_\infty$. Beyond $0.25x_r$, turbulent structures with smaller time scales and a downstream convection velocity of $0.57U_\infty$ generated most of the pressure fluctuations. Interestingly, the low-frequency wall-pressure signature typically associated with the flapping of the separated shear layer was found to be composed of standing and downstream/upstream propagating wave components. The latter seemed to originate from a point near the middle of the reattachment zone, suggesting the existence of an absolute instability of the *recirculation bubble*, which may be the cause of the flapping of the shear layer.

© 2003 American Institute of Physics. [DOI: 10.1063/1.1540633]

INTRODUCTION

Separating/reattaching flows produce large pressure fluctuations on the underlying surface. These fluctuations can cause significant vibration of the surface and subsequent generation of noise. To predict and/or control such vibration and noise effects one needs to understand the spatiotemporal character of the surface-pressure field. The present study addresses this issue through the use of a wall-microphone array to resolve the surface-pressure field both spatially and temporally in a basic separating/reattaching flow geometry. This provides further contribution to the bulk of the literature in this area, which has been primarily based on only one- or two-point measurements.

The flow geometry investigated consists of a splitter-plate attached to, and downstream of, a fence that is perpendicular to the flow, as shown in Fig. 1. This model was used because it has a separation bubble that is elongated in the streamwise (x) direction, and hence the development of the wall-pressure field within the bubble can be resolved properly using a sensor array with intersensor spacing that is not too small to realize. This also enabled measurements as close to the fence as $0.023x_r$, thus resolving a flow region that is typically not captured in the literature. Furthermore, in this geometry the boundary layer thickness is much smaller than the fence (step) height, and therefore the boundary layer de-

tails have minimal effect on the flow field within the reattachment zone.

Cherry *et al.*¹ made two-point unsteady surface pressure measurements in a separating/reattaching flow region. Their test model geometry was a blunt-face splitter plate, which is similar in nature to the splitter-plate-with-fence geometry. They demonstrated the convective nature of the surface-pressure imprint associated with the downstream motion of the shear layer structures through cross-correlation analysis between two signals from microphones spaced apart in the streamwise direction. Cherry *et al.*¹ also observed low- and high-frequency peaks in the power spectrum measured close to separation and near reattachment, respectively. They attributed the low-frequency signature to the flapping of the shear layer associated with the growth and decay of the separation bubble.

Farabee and Casarella² studied the fluctuating wall pressure in a forward- and backward-facing step flow. In the latter, Farabee and Casarella² found that close to separation the wall-pressure spectra showed the highest level of energy at lower frequencies; whereas, farther downstream, near reattachment, the highest level of energy was found at higher frequencies. Overall, the energy level increased in the downstream direction with the peak energy occurring around reattachment. This was a manifestation of the increase in the energy of the organized, turbulent structures as they convect downstream. A convection-velocity analysis showed that the pressure fluctuations close to separation were associated with the recirculating low-speed fluid and not the high-speed fluid

^{a)} Author to whom correspondence should be addressed. Electronic mail: naguib@egr.msu.edu

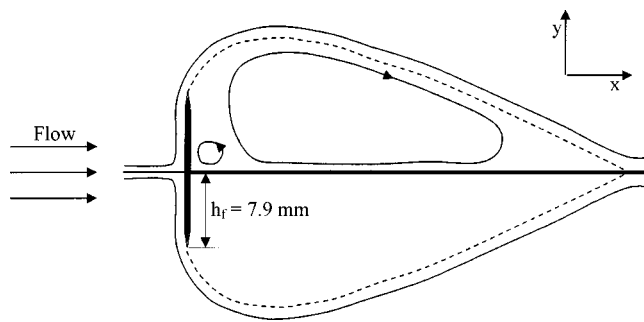


FIG. 1. Splitter-plate-with-fence geometry and ideal two-dimensional flow field: step height (h_f) = 7.9 mm and total fence height ($2H$) = 35 mm.

in the shear layer. However, Farabee and Casarella² commented that the convection velocity was *always* in the downstream direction, indicating that the pressure fluctuations were not originating from the reverse flow within the recirculation bubble.

Driver *et al.*,³ in their backward-facing-step study, noticed abnormal contraction and elongation of the separation bubble due to the shortening and lengthening of the reattachment length. This was labeled as the flapping motion of the shear layer with amplitude estimated to be 20% of the shear layer width. They used surface pressure measurements along with velocity measurements to show that there was a definite low frequency disturbance associated with the shear layer flapping, but that it contributed very little energy to the overall pressure fluctuations.

The two-paper sequence by Kiya and Sasaki^{4,5} provided an elaborate study of the wall pressure and its relation to the flow field in the reattachment zone over a splitter plate with a blunt leading edge. They found that at reattachment, the low-frequency pressure signature associated with shear layer flapping was predominantly out of phase with the signature near the separation point. Moreover, they reasoned that low-frequency positive pressure fluctuations at reattachment corresponded to inward movement of the shear layer while negative pressure fluctuations were the result of outward shear-layer movement. Kiya and Sasaki⁵ also demonstrated that valleys in the wall-pressure signal at reattachment were associated with a clockwise-rotating vortex that was located above the reattachment point. On the other hand, peaks in the signal were found beneath an “inrush” of high-energy irrotational fluid that was moving towards the wall. This inrush was located on the downstream side of the vortex structures associated with the negative pressure events.

Heenan and Morrison⁶ investigated wall-pressure fluctuations behind a rearward-facing step and passive control of these fluctuations using a permeable reattachment surface. Heenan and Morrison⁶ found an upstream convection velocity close to separation using cross-correlation and phase-angle analysis. They identified negative phase angles (with respect to a microphone signal measured immediately behind the step) at low frequencies and at locations from separation up to $0.4x_r$ in the impermeable case. This is the only study found to date that describes an upstream convection velocity.

Lee and Sung⁷ used a 32-microphone array downstream of a backward-facing step to measure wall-pressure fluctua-

tions in the streamwise and spanwise directions. Generally speaking, these investigators observed the same phenomenon in their experiment as experienced by earlier investigators of backward-facing-step studies. Notably, Lee and Sung⁷ found no evidence of an upstream convection velocity at low frequencies. Although in their convection velocity versus frequency plot, there were many singularities at low frequencies, which was not the case at higher frequencies.

The characteristics described thus far pertain to surface pressure measurement studies. A wealth of information has also been accumulated by authors that used different measurement techniques within similar types of flow geometries. In these separating/reattaching flow studies the measuring techniques used included hot-wire and pulsed-wire anemometry, skin-friction measurements, and particle image velocimetry. Of those, Castro and Haque,⁸ Eaton and Johnston,⁹ and Spazzini *et al.*¹⁰ are a few of the authors who also observed very large-scale, low-frequency motion close to separation and smaller-scale, higher-frequency motion close to reattachment. In all studies, the low-frequency signature was attributed to the flapping of the shear layer. On the other hand, Ruderich and Fernholz¹¹ and Chandrsuda and Bradshaw¹² are two of the handful of studies that found no evidence of such flapping.

EXPERIMENTAL SETUP

The present experiment was completed in the open-circuit, Subsonic Basic Research (Wind) Tunnel (SBRT) at NASA Langley Research Center in Hampton, Virginia. The wind tunnel has a 6:1 contraction upstream of a 0.57 m wide by 0.82 m high by 1.85 m long test section. For this study, the flow speed (U_∞) used was 15 m/s, resulting in a Reynolds number of 7900, based on the step height of the model (h_f , see Fig. 1). The corresponding free-stream turbulence intensity was less than 4%, which is higher than the fraction of a percent typically found in research facilities. Saathoff and Melbourne¹³ showed that increasing free-stream turbulence levels resulted in a decrease in the mean reattachment length (x_r) and an increase of the wall-pressure fluctuations. However, as will be seen in the Results and Discussion section, the overall characteristics of the mean and fluctuating wall-pressure field from the current study agrees quite well with the studies of Castro and Haque⁸ and Cherry *et al.*,¹ amongst others (e.g., see Figs. 3, 4, and 7 and related discussion). The free-stream turbulence intensity for both of these studies was on the order of 0.25% and 0.07%, respectively.

The design of the model, which was constructed out of aluminum, was symmetric with respect to top and bottom (Fig. 1). The total length of the model was $160h_f$ or $73H$ ($2H$ being the total fence height) and its width was $44h_f$ or $10H$. Endplates were placed on the sides of the splitter plate to improve the two dimensionality of the mean flow, according to Castro and Haque,⁸ resulting in a model aspect ratio of 36. The blockage ratio, as defined by Smits¹⁴ who found that the reattachment distance decreased with increasing blockage ratio, was around 2%. This resulted in a reattachment length of approximately 0.2 m ($25.6h_f$), which ensured that the reattachment point would be contained within the extent of

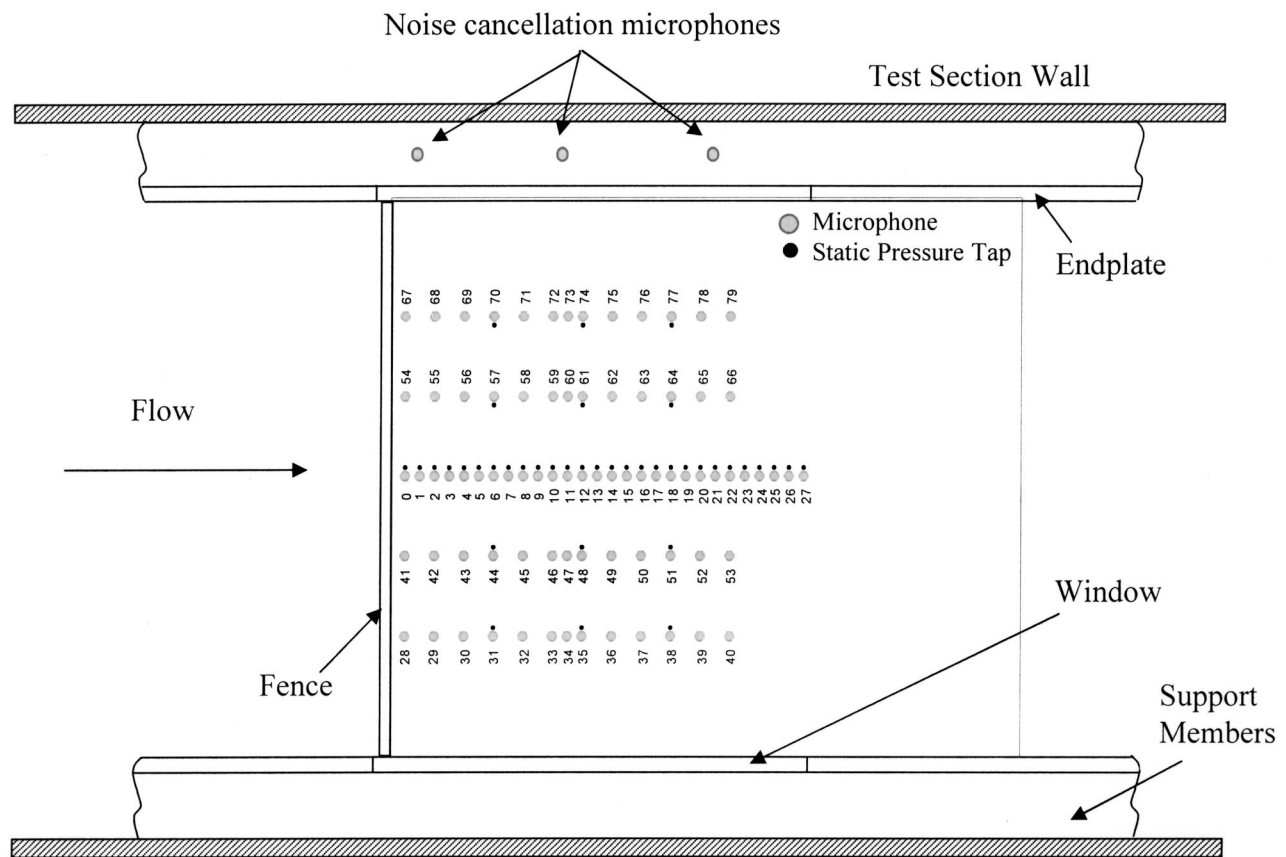


FIG. 2. Schematic detailing instrument plate layout and position of noise cancellation microphones.

the microphone array. The splitter plate was outfitted with 80 microphones and 80 static pressure taps. The configuration and numbering of the microphones and the static pressure taps are shown in Fig. 2.

The microphone array consisted of Panasonic (WM-60A) omnidirectional back electret condenser microphone cartridges with a bandwidth of 20–20 000 Hz. The microphones, each with a sensing diameter of 2 mm, were flush-mounted and were used to record the fluctuating pressure on the surface of the plate. The center row consisted of 28 microphones spaced $1.2h_f$ apart center to center in the streamwise direction, starting at $0.6h_f$ downstream of the fence. The current paper is focused on the analysis of these centerline microphones only.

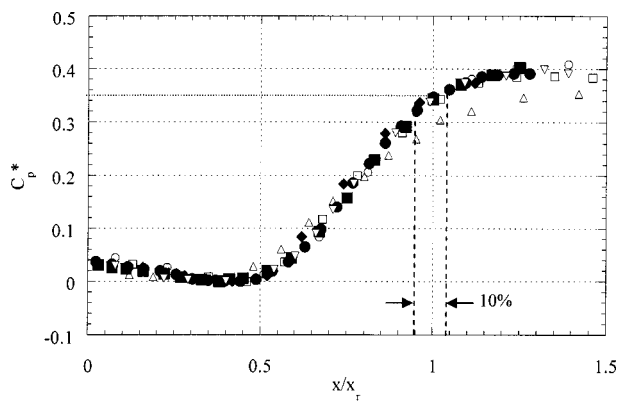
Each microphone was calibrated against a 0.25 in. B&K microphone up to 5 kHz. From the calibration, the sensitivity range of the microphones was determined to be 15 to 17.5 mV/Pa. The calibration results were also used to check matching of the phase characteristics of the microphones and to determine the microphone time delay. It was found that a typical microphone time delay ($\approx 10 \mu\text{s}$) was more than an order of magnitude (≈ 50 times) smaller than the average convection time between successive microphones ($635 \mu\text{s}$).

The outputs of the microphones were acquired using National Instruments A/D boards with maximum sampling rate of 19 531 Hz per channel. The corresponding time delay was $0.8 \mu\text{s}$ between successive channels, resulting in a $22.4 \mu\text{s}$ time delay between the most upstream and most downstream

microphones on the centerline. This delay, however, was about two orders of magnitude smaller than the period of the highest important frequency in the flow (most of the energy in the pressure fluctuations was contained in frequencies less than 200 Hz). Data for the experiment were sampled at 12 kHz for 15 seconds (about $1000x_r/U_\infty$), with the cutoff frequency of the antialiasing filters set at 5 kHz.

Generally speaking, microphone measurements are susceptible to contamination due to noise produced by the wind tunnel fan and disturbances caused by diffuser unsteadiness. In the current experiment, this was not a problem for most of the microphones since the pressure fluctuations produced in the separating/reattaching flow were significantly stronger than those associated with the background noise. However, to minimize tunnel-noise influences, the noise components associated with planar wave propagation through the tunnel were removed using the optimal-filtering approach from Naguib *et al.*¹⁵ The filtering technique was implemented with the aid of noise cancellation microphones, which were mounted outside the separating/reattaching flow region but at the same general streamwise location as the measurement microphones, as illustrated in Fig. 2.

Finally, the splitter plate was also instrumented with 40 static pressure taps on the top and bottom for a total of 80 taps. Static pressure measurements were primarily used to align the model in the tunnel and estimate the mean reattachment length. The location of the taps, which mirrored each other on top and bottom, is depicted in Fig. 2. The static



	Re	x_r/h_f or x/D	Blockage (%)
● Present Measurements	0.8×10^4	25.6	1.94
◆ Castro & Haque (1987)	2.2×10^4	19.2	6.2
■ Cherry, Hillier & Latour (1984)	3.2×10^4	4.9	3.79
○ Ruderich & Fernholz (1986)	1.4×10^4	17.2	10
□ Ruderich & Fernholz (1986)	0.9×10^4	22.6	5.7
△ Roshko & Lau (1965)	1.4×10^4	33.6	5
▽ Hillier, Latour & Cherry (1983)	1.4×10^4	23.9	2.5

FIG. 3. C_p^* distribution compared with six different studies.

pressure taps were coupled to a 48-port Scanivalve that was connected to a Setra 239 series pressure transducer. The transducer measured differential pressure in the range of 0–25.4 mm H₂O, outputting a corresponding 0–5 V signal.

RESULTS AND DISCUSSION

Mean-pressure distribution and reattachment length

The mean reattachment length (x_r) is an important parameter for the present flow geometry and, as shown by Ruderich and Fernholz,¹¹ appears to be the appropriate length scale for this flow field. Therefore, before analyzing the data the reattachment length was estimated for the purpose of normalizing the results. This was done utilizing the pressure coefficient (C_p^*) used by Ruderich and Fernholz¹¹ in their presentation of mean pressure results. The form of C_p^* was first proposed by Roshko and Lau.¹⁶ As Ruderich and Fernholz¹¹ explain, the mean pressure distribution data from different long-separation-bubble studies collapse well if plotted in the form C_p^* versus x/x_r , where $C_p^* = (C_p - C_{p,\min}) / (1 - C_{p,\min})$. C_p is defined as $(p_s - p_r) / (\frac{1}{2}\rho U_\infty^2)$; p_s is the time-mean surface pressure along the model, p_r is a reference pressure, measured at the exit of the contraction, $C_{p,\min}$ is the minimum C_p in the mean pressure distribution, and ρ is the fluid density. Figure 3 includes C_p^* distribution from six earlier investigations as a function of the distance along the splitter plate normalized by the reattachment length. All six studies, except Cherry *et al.*,¹ used a splitter-plate-with-fence configuration. Cherry *et al.*¹ investigated a blunt-face splitter plate, with the thickness of the plate denoted by D .

Although these studies were conducted at different Reynolds numbers and had various blockage ratios, resulting in a

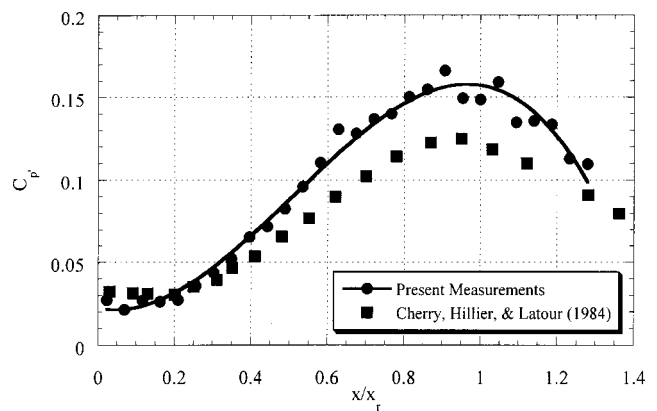


FIG. 4. Streamwise distribution of the coefficient of RMS pressure fluctuations.

difference in the reattachment lengths, the pressure distribution for all experiments correlate well when plotted using C_p^* versus x/x_r , even in the case of the blunt-face-splitter-plate geometry. Thus, a universal pressure coefficient (C_p^*) value may be found at the mean reattachment location ($x/x_r = 1$). This value was determined to be approximately $C_p^* = 0.35$. By applying this C_p^* value to the present data, the reattachment distance could be determined within $\pm 5\%$ uncertainty, based on the band of data scatter in Fig. 3. Therefore, the reattachment distance was determined to be roughly 205 mm or $25.6h_f$. Static pressure tap and microphone #21 are the ports closest to this reattachment value and thus their corresponding x location was used in the normalization of the present data throughout the study. The current $C_p^*(x/x_r)$ distribution obtained using this location as the reattachment length is included in Fig. 3. It is evident that with this determination of x_r , the current results agree quite well with the earlier investigations over the entire measurement range.

Fluctuating pressure distribution

The root-mean-square (RMS) coefficient of the pressure fluctuation ($C_{p'} = p'_{\text{rms}} / \frac{1}{2}\rho U_\infty^2$, where p' is the fluctuating pressure) is shown in Fig. 4 for the present study and that of Cherry *et al.*¹ Comparison with Cherry *et al.*¹ is done here because it is the only detailed study found with more than one-point unsteady surface pressure measurements in a separating/reattaching flow geometry similar in nature to the present experiment (i.e., one where the boundary layer thickness at separation is much smaller than the step height). Cherry *et al.*¹ conducted two-point measurements at different spacing on a thick splitter plate. Kiya and Sasaki⁴ also studied the flow state over a blunt-face splitter plate using extensive single- and two-point surface-pressure and velocity measurements. However, they displayed most of their data in velocity and velocity-pressure correlation plots. It should also be noted that although the study of Lee and Sung⁷ did utilize a 32-microphone array, their flow geometry was a backward facing step and not a splitter plate, with or without a fence. Overall, no study could be found that had the same specific flow geometry and more than one-point microphone measurements as used in this experiment.

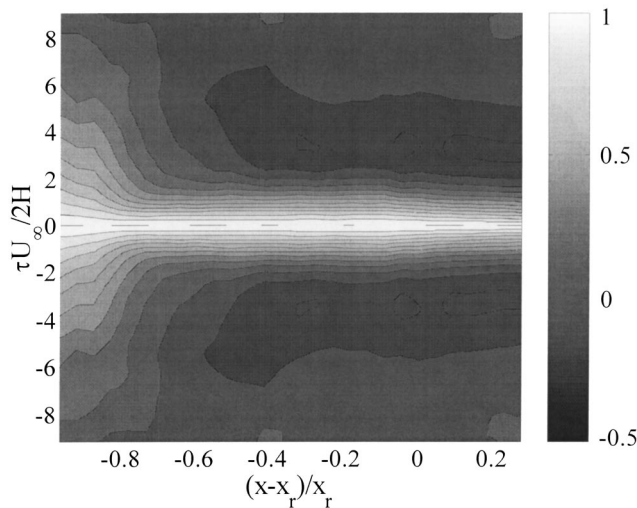


FIG. 5. Contour map of the autocorrelation coefficient for all 28 microphones along the centerline of the model.

The RMS data in Fig. 4 exhibit some scatter around the trend line, which is believed to be associated with the uncertainty of the microphone calibration procedure used to determine the sensitivity of the microphones. This uncertainty was found to be approximately 7%. Although, there is qualitatively good agreement between the two data sets in Fig. 4, there are some quantitative differences. In particular, the current $C_{p'}$ values are generally larger than those from Cherry *et al.*¹ (except very close to the separation point, where both sets agree). The difference between the two sets of results, which is largest in the vicinity of the peak in the $C_{p'}$ values, could be due to the difference in the model geometries selected for each study, or the higher free-stream turbulence intensity of the current study. It is important to note, however, that for both studies, the peak in $C_{p'}$ appears to be located slightly upstream of the mean location of the reattachment point.

Autocorrelation

To identify the dominant time scales in the wall-pressure time records, an autocorrelation analysis was conducted. The gray-scale contour map in Fig. 5 shows the autocorrelation coefficient ($R_{p'p'}$) for all 28 centerline microphones. The gray-scale bar indicates the values of the autocorrelation coefficient, which was obtained by normalizing the correlation function by the square of the RMS of the signal.

In the region immediately behind the fence, the autocorrelation function extent is wide and changes very little up to a distance of about $0.2-0.25x_r$ ($(x-x_r)/x_r = -0.80$ to -0.75) behind the fence. Farther downstream, this width narrows significantly over a relatively short distance [roughly from $0.25x_r$ to $0.5x_r$; $(x-x_r)/x_r = -0.75$ to -0.50] as demonstrated by the focusing of the $R_{p'p'}$ contours towards $\tau U_\infty/2H = 0$ line. Beyond this region, the contour lines remain approximately parallel to the constant τ lines showing very little change in $R_{p'p'}$ with additional increase in x . The region between $x/x_r = 0.25$ to 0.5 roughly delineates the start and end locations of the change in the

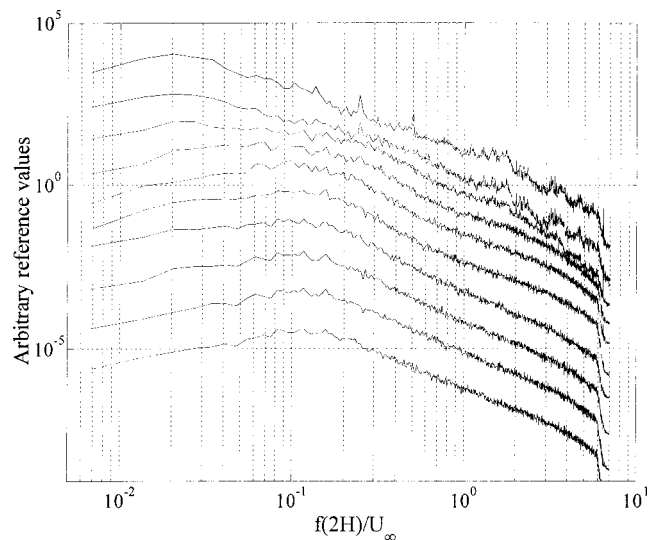


FIG. 6. Power spectra for selected microphones covering the measurement range—streamwise direction is from top to bottom.

time scales of the flow structures dominating $R_{p'p'}$. This region is referred to as the *changeover* region.

The dominance of large-time-scale (low-frequency) disturbances directly behind the fence has been identified in a number of studies. These include Castro and Haque,⁸ Cherry *et al.*,¹ Driver *et al.*,³ Eaton and Johnston,⁹ Farabee and Casarella,² and Lee and Sung.⁷ Some of these studies have attributed these disturbances to the flapping of the shear layer as discussed in the introduction. This flapping motion produces weak pressure fluctuations as depicted in Fig. 4 for the range $x < 0.25x_r$.

Farther downstream, the organized shear-layer structures grow in strength and move closer to the wall. This apparently is responsible for the increase in the RMS pressure fluctuation with downstream distance (Fig. 4). Moreover, these structures impose a shorter time scale than that encountered close to the fence on the autocorrelation function. Thus, the increasing influence of these structures on the wall pressure appears to be responsible for the observed change in the $C_{p'}$ and $R_{p'p'}$ character within the changeover region. Past this region, in the vicinity of the reattachment location and farther downstream, the energy of the shear layer organized structures appears to saturate (as suggested by the RMS plot in Fig. 4). This is possibly why no substantial change in $R_{p'p'}$ is detected past the changeover zone.

Power spectra

The power spectrum at every third microphone along the centerline is shown in Fig. 6. Except for the spectrum at the most upstream location, each spectrum plot is shifted along the ordinate by an integer number of decades in order to display the plots without clutter. Close to separation, the peak in the power spectrum is seen to be roughly around $f(2H)/U_\infty = 0.02-0.03$ ($fx_r/U_\infty = 0.12-0.18$), which is approximately the same value reported by Cherry *et al.*¹ In the case of the backward-facing step, Lee and Sung⁷ also found a similar peak frequency value close to separation at

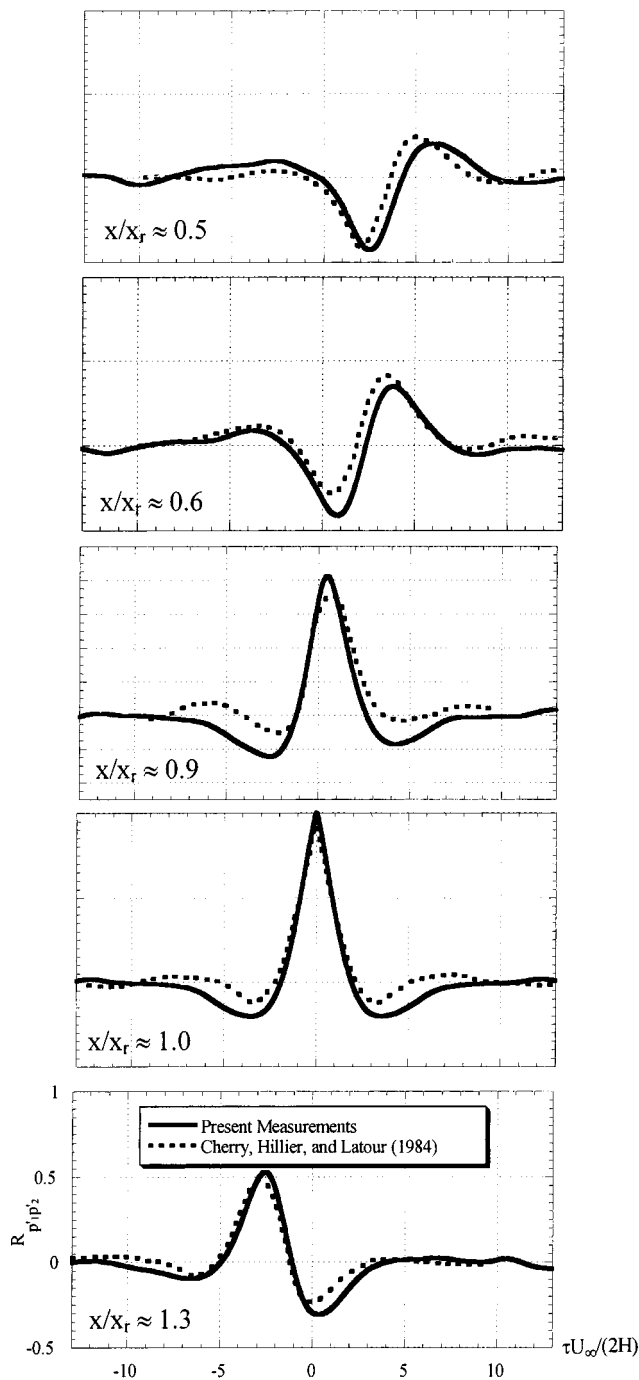


FIG. 7. Cross-correlation results at five different locations compared to data from Cherry *et al.* (Ref. 1).

$fH/U_\infty=0.015$ (H =the height of the step), which when scaled by x_r instead gives a value of $fx_r/U_\infty=0.11$. This is comparable to the values given by Spazzini *et al.*,¹⁰ $fx_r/U_\infty=0.08$, and Heenan and Morrison,⁶ $fx_r/U_\infty=0.1$. Cherry *et al.*¹ along with Heenan and Morrison,⁶ Driver *et al.*,³ and Lee and Sung,⁷ have associated this low-frequency peak with the flapping of the shear layer. Farabee and Casarella² also indicated that the wall pressure fluctuations close to separation were caused by the unsteadiness of the low-speed recirculating flow, rather than the highly turbulent structures in the shear layer.

TABLE I. Microphone positions used in cross-correlation analyses.

	Present study— x/x_r	Cherry <i>et al.</i> — x/x_r
1	0.54	0.55
2	0.65	0.70
3	0.95	0.95
4	1.0	1.0
5	1.3	1.4

Farther downstream, the energy in the spectrum is located at higher frequencies in the range $f(2H)/U_\infty=0.1-0.15$ ($fx_r/U_\infty=0.6-0.9$), which is in agreement with the findings of Cherry *et al.*,¹ where the frequency is normalized using the thickness of the splitter plate in their case. Lee and Sung⁷ stated that the power spectrum reaches a maximum at $fH/U_\infty=0.068$, or $fx_r/U_\infty=0.5$. Spazzini *et al.*¹⁰ found the spectral peak at $fx_r/U_\infty=1.0$ along with Heenan and Morrison.⁶ Driver *et al.*³ recorded a peak at $fx_r/U_\infty=0.6$ close to reattachment. This higher frequency peak has been attributed to the vortical structures within the shear layer.

Cross-correlation and phase angle analysis

Prior to presenting results for all 28 microphones, the consistency of the current measurements with data from the literature was examined. To this end, the cross-correlation coefficient obtained from five different microphones correlated with the microphone closest to reattachment was calculated using the equation: $R_{p_1'p_2'} = \overline{p_1'(x_r, t)p_2'(x, t - \tau)} / p_{1,rms}'p_{2,rms}'$; where the overbar denotes time averaging. The outcome is compared to similar results from Cherry *et al.*¹ in Fig. 7 for the x locations listed in Table I. Note that the results obtained for the microphone at $x/x_r=1$ represent the autocorrelation function. The current data compare well with the data from Cherry *et al.*,¹ who characterize the data as a manifestation of “clear convective motion in the mainstream direction.” The convective motion is implied from the shift in the location of the correlation peak for microphones located at different x positions. A more detailed picture of the spatial structure of the cross correlation may be obtained by making use of all microphones.

Figure 8 shows a gray-scale contour map of the cross-correlation coefficient of the signals from all microphones with that from the microphone closest to reattachment. In the cross-correlation contour map, there are three distinct features. One feature is a set of positive contour lines that are centered around the origin of the plot. These contour lines have the shape of a ridge or lobe that is inclined at a negative angle. The locus of the peaks along the lobe (shown in the figure using a broken line) represents the time delay (say τ^*) at which the cross correlation is a maximum for different x locations. Clearly, the peak correlation at a location downstream of x_r , say x^* , is found by delaying the signal recorded at the downstream location (corresponding to a negative τ) with respect to that measured at x_r . This delay represents the *average* time for flow structures to travel from x_r to x^* and generate a similar (correlated) wall pressure

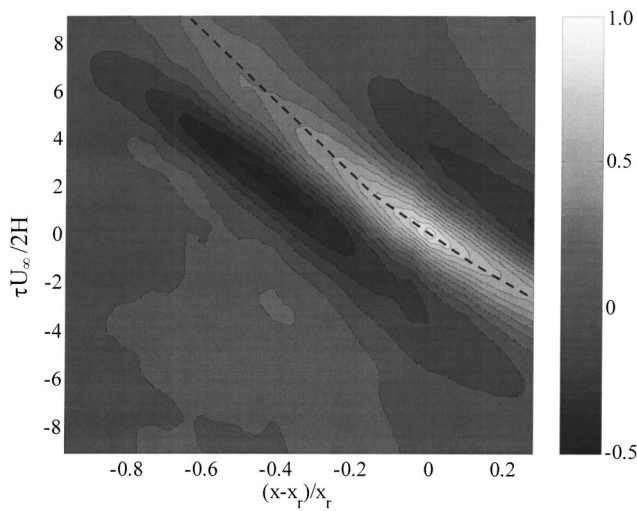


FIG. 8. Cross-correlation-coefficient color contour map for all 28 centerline microphones (reference microphone closest to reattachment).

signature. Thus, by calculating the slope of the peak-locus line, or $(d\tau^*/dx)^{-1}$, one may estimate the average convection speed (U_c) of the dominant flow structures. Note that, as discussed above, convection velocities in the downstream direction are associated with negatively inclined lobes.

The other two distinct features are the two negatively inclined lobes that represent negative cross-correlation peak locations. These negative peaks give the time delay to the highest negative correlation. Thus, the slope of the locus of the main positive (or negative) peaks could be used in estimating U_c . This slope was found by approximating the peak locus of the positive lobe with a straight-line fit, giving $U_c = 0.57U_\infty$. Heenan and Morrison⁶ reported convective velocities ranging between $0.5U_\infty$ and $0.6U_\infty$ depending on the position along the model. Lee and Sung⁷ stated that convective velocities at high frequencies converged to a value of

$0.6U_\infty$ in their backward-facing-step study, while Cherry *et al.*¹ determined the convective velocity to be $0.5U_\infty$. Generally, U_c values were cited to range from 0.5 to 0.6 of the free-stream velocity in the literature, depending on model geometry, location of measurement, and measuring technique.

The cross-correlation results yield an average convection velocity associated with various time scales. In order to determine the convection velocities associated with individual time scales (frequencies), the streamwise development of the phase angle (θ) was examined for various frequencies. θ at a given frequency and x location is computed from the cross spectrum between the microphone at that x location and a reference microphone (closest to the fence in the current results).

Figure 9 displays a plot of the phase angle as function of $(x-x_r)/x_r$ for three different frequencies. The frequencies were selected such that the same amount of energy was captured on either side of the high frequency peak ($f(2H)/U_\infty \approx 0.12$), which was determined from the power spectrum. Therefore, the three frequencies used in the phase plot were $f(2H)/U_\infty = 0.05, 0.12,$ and 0.30 , which mark the beginning, middle, and end of the region of frequencies containing most of the energy in the spectra for x greater than approximately $0.25x_r$. Also note that data in Fig. 9 are plotted starting from $x \approx 0.25x_r$, which as indicated earlier is believed to be the location at which the signature of the shear layer vortices starts to get stronger with downstream distance and dominate the wall-pressure fluctuations.

In Fig. 9, the phase data reveal a steady, linear-like increase of the phase angle in the downstream direction. The slopes of these lines differ, depending on the frequency. The convective velocity can be calculated from $U_c = 2\pi f x_r / (\Delta\theta/\Delta x)$; where $\Delta\theta/\Delta x$ is the slope of the phase plot (obtained from a least-squares line fit). The resulting convection velocities for the different frequencies are given

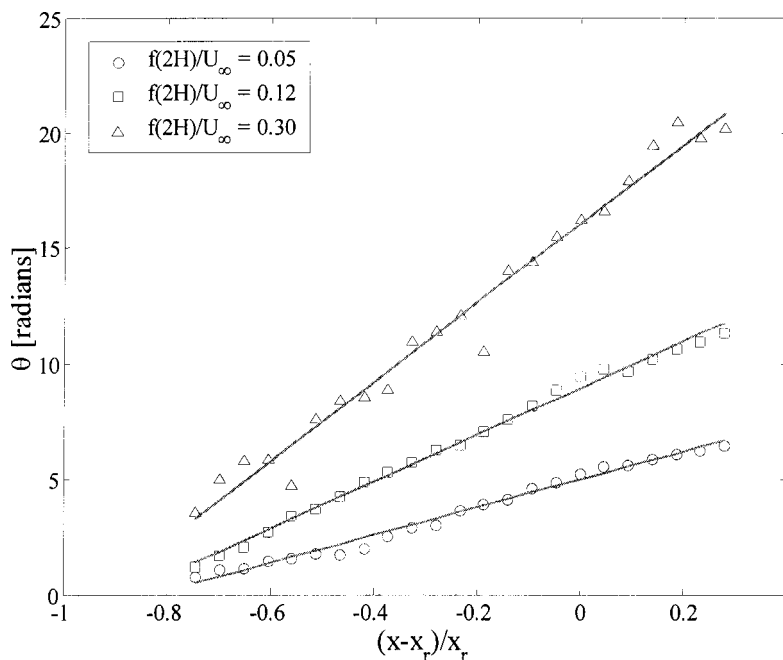


FIG. 9. Streamwise development of the phase angle for three different frequencies [reference microphone at $(x-x_r)/x_r = -0.98$].

TABLE II. Downstream convective velocities for various frequencies.

$f(2H)/U_\infty$	U_c/U_∞
0.05	0.33
0.12	0.44
0.30	0.64

in Table II, where it is found that low frequency disturbances travel at a lower speed than higher frequency ones.

In the cross-correlation results in Fig. 8, no positively inclined lobes are depicted, and hence there is no evidence of negative (upstream) convection velocity as reported by Heenan and Morrison.⁶ Lee and Sung⁷ also found no evidence of this phenomenon in their study. However, since the results of Heenan and Morrison⁶ show negative U_c values at x locations that are close to the step, it was decided to explore the convective characteristics of the surface pressure at locations closer to the fence. To this end, the cross-correlation function for all 28 microphones relative to microphone #5 (which is located at $x/x_r \approx 0.25$) was calculated and plotted in Fig. 10.

From the contour plot, an inclined positive lobe is found on either side of the high correlation coefficient peak at microphone #5. These two lobes have opposite signed slopes with respect to each other. This provides evidence that there are two convection velocities: one upstream and one downstream as suggested earlier by Heenan and Morrison.⁶ Additionally, the evidence of the downstream-traveling disturbances in Fig. 10 shows that these disturbances are detectable as early as microphone #5, or $x \approx 0.25x_r$. Therefore, it is reasoned that the flow structures seen to dominate the measurements closer to reattachment are first noticeable in the surface pressure measurements around the $0.25x_r$ distance, as hypothesized earlier based on the RMS and auto-correlation results.

On the other hand, the footprint of the upstream-propagating disturbances in Fig. 10 (the positive-inclined

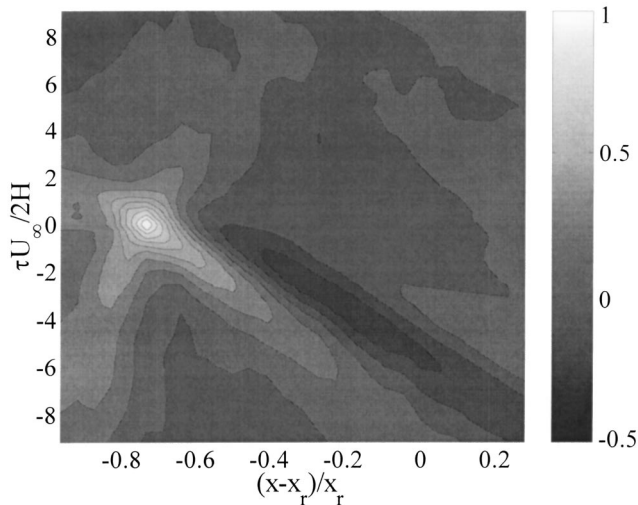


FIG. 10. Cross-correlation-coefficient contour plot for all 28 microphones [reference microphone at $(x-x_r)/x_r = -0.74$].

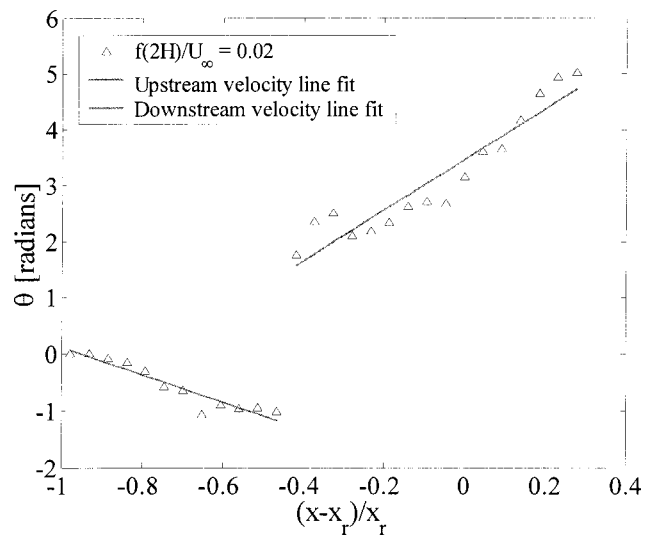


FIG. 11. Phase angle plot for $f(2H)/U_\infty \approx 0.02$.

lobe) seems to extend to x/x_r of approximately 0.5 before fading away. The upstream convection velocity associated with this lobe was determined to be 21% of U_∞ . This is similar to the value determined by Heenan and Morrison.⁶ Their value was about 20% of U_∞ . The downstream convection velocity was also calculated using the results in Fig. 10 to be 47% of U_∞ . This value is lower than the 57% U_∞ calculated earlier from the cross-correlation map with the reference microphone located closest to reattachment (Fig. 8). This suggests that the convection velocity magnitude increases with downstream distance. Heenan and Morrison⁶ also noticed this trend in their impermeable backward-facing step. Upstream near the fence, they observed a $0.5U_\infty$ convection velocity that increased to $0.6U_\infty$ close to reattachment and continued to rise farther downstream.

Because the above results depict upstream-traveling wall-pressure fluctuations in the region near the fence, where $f(2H)/U_\infty \approx 0.02$ is the dominant frequency, it was decided to explore the phase characteristics relative to microphone #0 at this frequency value. The results are given in Fig. 11. Consistent with the cross-correlation observations, the phase data exhibit a negative slope in a region extending approximately to $x = 0.5x_r$, indicating an upstream convection velocity in this region. The specific U_c value was calculated from the slope of a linear fit to the data to be $-0.31U_\infty$, which is larger than the value calculated from the cross-correlation results. A possible explanation for this discrepancy will be discussed below.

Farther downstream, a switch to positively inclined phase characteristics indicates a downstream convection velocity. This does not necessarily indicate the confinement of the upstream-propagating disturbances to the zone $x < 0.5x_r$. In particular, the phase results associated with backward propagation of disturbances at locations downstream of $0.5x_r$ may be masked by those associated with more energetic downstream motion at the same frequency. This is an important issue that will be addressed further in the next section.

The most surprising result in Fig. 11 is the phase angle

jump of about π at the point where the phase versus x behavior switches from a negative to positive sloped line. It is emphasized here that this jump is not the result of a phase unwrapping problem. In particular, the phase determination algorithm used here enables angle calculation in the range $-\pi < \theta \leq \pi$; i.e., the phase angle is ambiguous within integer multiples of 2π rather than π . If one does make -2π correction to the results in Fig. 11, the phase jump will change from positive to negative but will not disappear.

The observed phase step change of π is reminiscent of that associated with a standing-wave-like disturbance. Interestingly, Kiya and Sasaki⁵ suggested that the low-frequency wall-pressure unsteadiness associated with the shear-layer flapping might be approximated by a standing wave with a node near the middle of the reattachment zone. Kiya and Sasaki⁵ were able to rationalize the standing-wave character of the low-frequency wall-pressure fluctuations by considering the stretching and compression, in the x direction, of the mean-pressure distribution (see Fig. 3) in response to the shear-layer flapping. For locations upstream of the broad negative peak located around $x/x_r=0.5$, the pressure would increase with stretching of the profile, while for locations downstream of the peak, the pressure would decrease. Thus, one would expect fluctuations in the wall-pressure upstream of $x=0.5x_r$ to be out of phase from those farther downstream, and hence the standing-wave character. The phase jump of π in the current results provides convincing evidence of the standing-wave character of the wall-pressure fluctuations associated with shear-layer flapping.

From qualitative inspection of time series, Cherry *et al.*¹ also noticed an antiphase relation between the low-frequency wall-pressure signal measured at reattachment and that measured at $x/x_r=0.27$. Moreover, they found a negative correlation coefficient of -0.15 between the wall-pressure measurements at the two locations. Lee and Sung⁷ associated the flapping frequency with a stationary ($k_x=0$; where k_x is the streamwise wave number) spatial mode. It is hypothesized here that Lee and Sung's^{7,17} $k_x=0$ mode represents the instantaneous streamwise average of the standing wave (which has a nonzero streamwise wave number), and hence they are both a manifestation of the shear-layer flapping.

Finally, it is recalled here that the phase results at the flapping frequency also depict upstream/downstream traveling disturbances (Fig. 11). Whereas a reasonable physical argument could be made for the association of the shear-layer flapping with the standing-wave component of the phase plot, no such association is readily obvious for the propagating modes. However, it is believed that the coexistence of the stationary and propagating modes is responsible for the overestimation of the magnitude of the upstream convection velocity from the phase results, in comparison to that obtained from the cross-correlation results. More specifically, the convection speed of a standing wave is infinite (as would be determined from the slope of the phase line of such a wave). Since the observed phase results are affected by both standing and propagating disturbances, the estimated convection velocity would be a weighted average of both, which would tend to overestimate the magnitude of the convection speed of the propagating mode. In the following, the nature

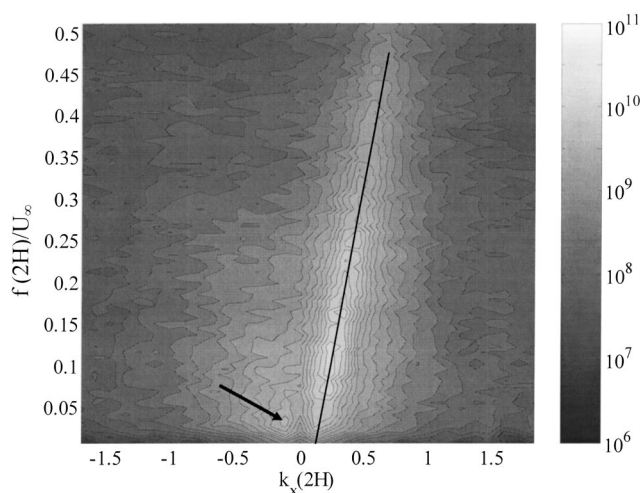


FIG. 12. Frequency-wave-number spectrum for all 28 microphones.

of the propagating modes at the flapping frequency is explored further using a frequency-wave-number spectrum analysis.

Frequency-wave-number spectrum

The frequency-wave-number ($f-k_x$) spectrum is obtained from the two-dimensional Fourier transformation of the autocorrelation of the space-time wall-pressure signal ($p'(x,t)$). As a result, this spectrum decomposes the energy content of the wall-pressure field into contributions at different frequency and wave-number combinations. Figure 12 shows a gray-scale contour plot of the frequency-wave-number spectrum with the gray-scale bar indicating the magnitude of the spectrum on a logarithmic scale. Depicted in the plot is a concentration of energy in a ridge of peak spectrum values inclined at an angle and located in the right half plane, or $k_x > 0$. The peak locus of this ridge is practically linear and approximately, but not exactly, passes through the origin of the plot. Since the convection speed at a given f and k_x point is the slope of a straight line drawn from the origin of the $f-k_x$ spectrum to the point, the ridge represents downstream (positive) traveling disturbances.

The small offset between the origin and the intercept of the peak locus with the k_x axis results in frequency (wave number) dependent convection velocities for different points along the ridge. These convection velocities were calculated by determining the equation of a least-squares line fit to the ridge (seen in Fig. 12) and dividing through the frequency to obtain the convection velocity as a function of frequency. Figure 13 shows a plot of the results compared to the data based on the phase angle plot (Fig. 9 and Table II) for comparison purposes. The convection velocities from the phase angle plot follow the $f-k_x$ spectrum results curve within $\pm 5-10\%$. The difference may be the result of the fact that, at a given frequency, the $f-k_x$ spectrum results filter out any contributions from wave numbers that are not part of the convective ridge. The phase data, on the other hand, are inevitably contaminated by wave numbers that may not be part of the convective motion.

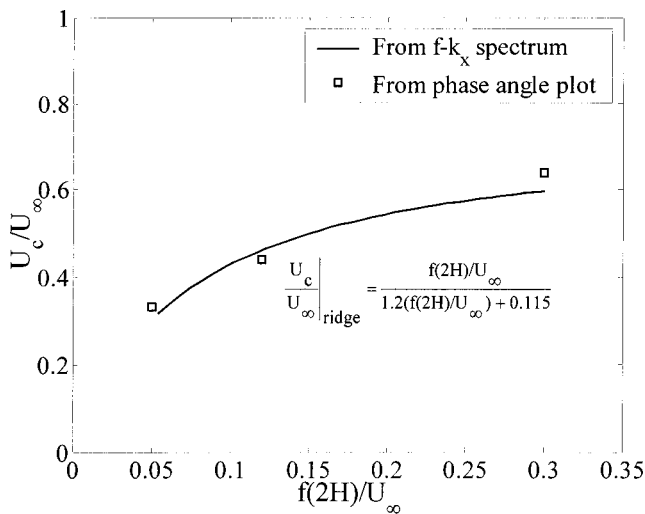


FIG. 13. Normalized convection velocity as a function of normalized frequency.

On the other hand, at negative wave numbers, an isolated peak (shown by an arrow in Fig. 12) in the $f-k_x$ spectrum is visible in the lower frequency range at $f(2H)/U_\infty \approx 0.02$ and $k_x(2H) \approx 0.11$, indicating an upstream convection velocity of $U_c \approx 0.21U_\infty$ as found in the cross-correlation results earlier. Lee and Sung⁷ also computed a frequency-wave-number spectrum similar to the one in Fig. 12. Their results show a ridge associated with a downstream convection velocity as well as a stationary mode along the $k_x=0$ axis, but they did not observe an upstream convection velocity as previously mentioned. It is believed that Lee and Sung⁷ could not find a negative convection speed because their upstream most measurement location extended down to only $x/x_r \approx 0.27$. Similarly, the measurements of Farabee and Casarella,² who also reported no upstream convection velocity, were limited to $x/x_r > 0.25$. As seen in the current study, the strongest manifestation of the upstream propagating disturbances is in the region $x/x_r < 0.25$.

Unlike the phase results in Fig. 11, where all disturbances at $f(2H)/U_\infty \approx 0.02$ influence the estimated phase at that frequency, the $f-k_x$ spectrum analysis can be used to separate contributions by the upstream traveling disturbances from those traveling downstream. It was decided to capitalize on this property to investigate further whether the upstream traveling disturbances associated with the local peak at $f(2H)/U_\infty \approx 0.02$ and $k_x(2H) \approx 0.11$ are also found downstream of $x/x_r \approx 0.5$ (or phase jump point in Fig. 11). Therefore, the $f-k_x$ spectrum was calculated from the first 16 microphones (covering $0.02 < x/x_r < 0.72$) and contrasted with that obtained from the last 16 microphones (spanning $0.58 < x/x_r < 1.3$). Figure 14 depicts the frequency-wave-number spectrum for the first 16 microphones located closest to separation. The results indicate that within the first 16 microphones there is evidence of both an upstream and downstream convection velocity, as expected.

In Fig. 15, the $f-k_x$ spectrum for the last 16 microphones (containing the reattachment area) is shown. In this spectrum, only the inclined ridge at positive wave numbers appears. The localized peak at the negative wave number of

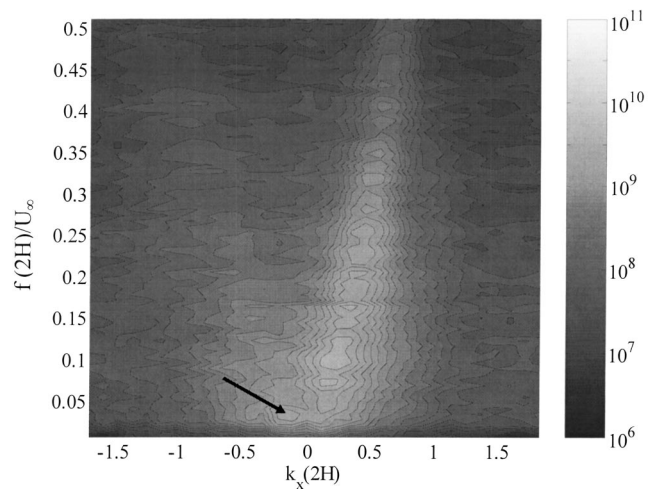


FIG. 14. Frequency-wave-number spectrum for the first 16 microphones located closest to the fence.

$0.11/(2H)$ is not visible. This provides compelling evidence that the most energetic upstream traveling disturbances of $f(2H)/U_\infty \approx 0.02$ are confined in the range $x < 0.5x_r$, as suggested by Fig. 11, but only properly verified here. It should be noted, however, that broadband relatively weak spectrum values are observed in the negative k_x plane in all $f-k_x$ spectrum results. These are believed to be associated with background turbulence/flow-disturbances propagating from the reattachment point towards the fence.

FURTHER DISCUSSION

The above discussion suggests that the traveling wall-pressure disturbances at $f(2H)/U_\infty \approx 0.02$ originate from a point around the middle of the recirculation zone and propagate in both the upstream and downstream directions. That is, those fluctuations *do not* represent disturbances that are carried by the reversed flow near the wall from the reattachment point towards the fence, or step. The notion of upstream and downstream traveling disturbances originating

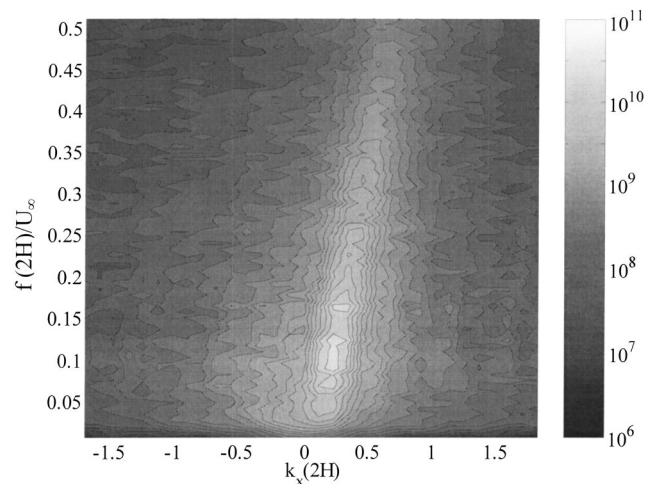


FIG. 15. Frequency-wave-number spectrum of the last 16 microphones along the center line containing the reattachment region.

from a common source location alludes to the existence of an absolutely unstable flow region in the middle of the recirculation zone [see the classic paper by Huerre and Monkewitz¹⁸ (1990) for detailed account of local and global instability concepts].

Recently, Wee *et al.*¹⁹ used a composite hyperbolic-tangent function to model the mean velocity profile downstream of a sudden expansion in a channel flow. They conducted a local stability analysis of the model velocity profile and found that for a sufficiently large reverse flow component within the reattachment region, the model flow became absolutely unstable. Furthermore, they were able to show that the largest temporal growth rate of the absolute instability was located near the middle of the recirculation zone. These findings are consistent with the current observation of a disturbance source near the middle of the recirculation zone that produces upstream and downstream traveling disturbances at $f(2H)/U_\infty \approx 0.02$. This frequency, however, is almost seven times smaller than the predicted frequency of the most amplified mode by Wee *et al.*,¹⁹ when both frequencies are normalized based on the step (fence) height. In fact Wee *et al.*¹⁹ associates the absolute instability with vortex shedding from the separation bubble, whereas the lower frequency of $f(2H)/U_\infty \approx 0.02$ is that commonly associated with shear-layer flapping.

Convincing evidence that possible instability associated with the back flow in the separation bubble would relate to the lower-frequency shear-layer flapping rather than the vortex shedding from the reattachment zone may be found in the study of Heenan and Morrison.^{6,20} These authors utilized a porous reattachment surface to practically eliminate the back flow within the separation bubble. The weakening of the back flow was associated with the elimination of the low-frequency wall-pressure peak associated with the shear-layer flapping. On the other hand, Heenan and Morrison⁶ found the dominant high-frequency peak in the wall pressure spectrum near reattachment to remain unchanged in frequency but experienced a small attenuation in energy. Since this frequency is the one associated with the passage of the shear layer vortices, Heenan and Morrison's⁶ results seem to conclusively demonstrate that the weakening or elimination of the back flow in the recirculation zone stabilizes the shear-layer flapping while not affecting the shear-layer vortex shedding substantially.

The source of the discrepancy in the frequency value predicted by Wee *et al.*¹⁹ and that associated with shear-layer flapping is not clear, although limitations of parallel flow assumption in the instability calculation may affect the prediction of the frequency value. Notwithstanding this limitation, it is believed that the analysis of Wee *et al.*¹⁹ is very significant in showing that a mean-velocity profile representative of the recirculation zone of separating/reattaching flows is capable of supporting absolute instability for sufficiently strong reversed flow.

Conceptually, the mean flow downstream of the fence, or a backward-facing step, may be viewed to be primarily composed of two components: a separating shear layer and a recirculating flow. In this respect, the recirculating flow possesses both a forward and backward flow components that

are essential to the absolute instability of the model velocity profile of Wee *et al.*¹⁹ In fact, the backward flow component is an entity of the recirculation bubble rather than the shear layer itself. Hence, it is proposed here that a plausible alternate interpretation of Wee *et al.*¹⁹ analysis is that it provides evidence for the existence of an absolute instability of the *recirculation bubble*, independent of the *shear layer* and its subsequent reattachment. The source of this instability is located near the middle of the recirculation zone, from which upstream and downstream propagating disturbances emanate. This instability causes the flapping of the shear layer, and hence it has the same frequency as that traditionally associated with the flapping motion and found practically in all wall-pressure (see Introduction) and wall-shear (e.g., Spazzini *et al.*¹⁰) measurements. Presumably, the instability of the shear layer itself is not totally independent of the bubble instability. One could imagine that the flapping of the shear layer modulates the shear layer instability process, affecting to some degree the growth and development of the shear-layer vortices on instantaneous bases. Evidence for such modulating influences has been reported by Lee and Sung,¹⁷ Heenan and Morrison,⁶ Kiya and Sasaki,⁵ and Cherry *et al.*¹

The proposition of an absolute instability of the recirculation bubble as the origin of the shear-layer flapping appends another hypothesis to an existing list of scenarios. Eaton and Johnston⁹ suggested that the shear-layer unsteadiness was produced by an instantaneous imbalance in the fluid entrained by the shear layer from the recirculation zone and that reinjected at reattachment. Kiya and Sasaki⁴ proposed that the flapping motion was caused by intermittent shedding of very large vortical structures from the recirculation bubble. These structures were formed by accumulation of vorticity within the bubble to a point where a large vortex was shed and the bubble collapsed, leading to an inward movement of the shear layer. It may be possible that the Kiya and Sasaki⁴ proposition is in fact a physical description of the flow pattern associated with the absolute instability proposed here. Although, it seems doubtful that the growth and collapse of the bubble is associated with vortex shedding since the highest concentration of pressure-fluctuation energy in the downstream convecting disturbances is found at $f(2H)/U_\infty = 0.1-0.15$, which is significantly higher than the flapping frequency.

More recently, Spazzini *et al.*¹⁰ conjectured that the flapping of the shear layer was associated with a cycle of growth and decay of the *secondary* (corner) recirculation bubble. It was found that when the bubble grew to a size comparable to the step height, it broke down leading to a collapse of the organized flow pattern, including vortex formation in the shear layer, and the start of a new cycle of growth/decay of the bubble. The flow events described by Spazzini *et al.*¹⁰ could very well be consistent with the growth and collapse of the *main* recirculation bubble proposed by Kiya and Sasaki,⁴ since each pertains to a different region in the flow.

Other hypotheses concerning the origin of flapping relate to feedback of disturbances from the reattachment point to the upstream separation point. These have been suggested by Mabey²¹ and Castro and Haque.⁸ However, the current re-

sults seem to downplay these hypotheses, by showing that the strongest feedback disturbances at the flapping frequency originate from the center of the recirculation zone rather than the reattachment point.

It should be mentioned here that the idea of an absolutely unstable recirculation bubble that produces shear-layer flapping and modulates the shear layer instability is not at odds with the mechanisms of instability of the shear layer itself proposed by Sigurdson²² and Kiya *et al.*²³ Sigurdson²² demonstrated that the passage frequency of the terminal vortices of the separating/reattaching shear layer over a blunt cylinder, and related configurations, is related to a shedding type instability mechanism resulting from the interaction of the vortices with their images when they approach the wall. Sigurdson likened this instability to that associated with the Von Karman vortex shedding in the wake of a cylinder.

On the other hand, Kiya *et al.*²³ attributes the selectivity of the shedding frequency to the existence of an acoustic feedback loop, whereby the shear-layer vortices impinging on the wall at reattachment produce disturbances that travel upstream at the speed of sound and modify the roll-up of the shear layer near the separation point. Since both points of view pertain to the shear layer itself and its interaction with the wall, they appear to be of no contradiction to the proposed recirculation flow instability as the source of shear-layer flapping. In fact, the insensitivity of the vortex shedding frequency to substantial weakening of the reverse flow, as found by Heenan and Morrison⁶ and discussed above, provides a strong evidence for the fair amount of independence of the vortex shedding instability from the proposed recirculation bubble instability.

CONCLUSIONS

Overall, two distinctive regions emerged from the spatiotemporal analysis of the surface pressure measurements. Upstream, from the fence to $0.25x_r$, the surface-pressure signature was dominated by large-time-scale disturbances and an *upstream* convection velocity of $0.21U_\infty$. Beyond $0.25x_r$, turbulent structures with smaller time scales and a downstream convection velocity of $0.57U_\infty$ generated most of the pressure fluctuations. Transition between the two different time scales occurred in a fairly short region extending from $0.25x_r$ to $0.5x_r$.

Evidence is found for the existence of an absolute instability zone, or self-sustained oscillator, near the middle of the recirculation zone. This self-sustained oscillator, which is the result of the instability of the recirculation flow within the separation bubble, continuously drives the separation bubble into states of expansion and contraction leading to shear-layer flapping and possible modulation of its instability process. This proposition raises further questions relating to more detailed characterization of the bubble absolute instability and its independence of the shear layer and its reattachment, the physical nature of the shear-layer modulation process by the bubble instability, and the influence of this modulation on the shear layer instability characteristics and subsequent vortex formation.

ACKNOWLEDGMENTS

This work was supported under a grant (NGT-1-52216) through the Graduate Student Research Program, which was sponsored by the Advanced Measurement and Diagnostics Branch at NASA Langley Research Center in Hampton, Virginia. The authors would also like to thank Scott M. Bartram for his hard work in setting up the equipment for the project.

- ¹N. J. Cherry, R. Hillier, and M. E. M. P. Latour, "Unsteady measurements in a separated and reattaching flow," *J. Fluid Mech.* **144**, 13 (1984).
- ²T. M. Farabee and M. J. Casarella, "Measurements of fluctuating wall pressure for separated/reattached boundary layer flows," *Trans. ASME, J. Vib., Acoust., Stress, Reliab. Des.* **108**, 301 (1986).
- ³D. M. Driver, H. L. Seegmiller, and J. G. Marvin, "Time-dependent behavior of reattaching shear layer," *AIAA J.* **25**, 914 (1987).
- ⁴M. Kiya and K. Sasaki, "Structure of a turbulent separation bubble," *J. Fluid Mech.* **137**, 83 (1983).
- ⁵M. Kiya and K. Sasaki, "Structure of large-scale vortices and unsteady reverse flow in the reattaching zone of a turbulent separation bubble," *J. Fluid Mech.* **154**, 463 (1985).
- ⁶A. F. Heenan and J. F. Morrison, "Passive control of pressure fluctuations generated by separated flow," *AIAA J.* **36**, 1014 (1998).
- ⁷I. Lee and H. J. Sung, "Characteristics of wall pressure fluctuations in separated and reattaching flows over a backward-facing step: Part I. Time-mean statistics and cross-spectral analyses," *Exp. Fluids* **30**, 262 (2001).
- ⁸I. P. Castro and A. Haque, "The structure of a turbulent shear layer bounding a separation region," *J. Fluid Mech.* **179**, 439 (1987).
- ⁹J. K. Eaton and J. P. Johnston, "A review of research on subsonic turbulent flow reattachment," *AIAA J.* **19**, 1093 (1981).
- ¹⁰P. G. Spazzini, G. Iuso, M. Onorato, N. Zurlo, and G. M. Di Cicca, "Unsteady behavior of back-facing step flow," *Exp. Fluids* **30**, 551 (2001).
- ¹¹R. Ruderich and H. H. Fernholz, "An experimental investigation of a turbulent shear flow with separation, reverse flow, and reattachment," *J. Fluid Mech.* **163**, 283 (1986).
- ¹²C. Chandrsuda and P. Bradshaw, "Turbulence structure of a reattaching mixing layer," *J. Fluid Mech.* **110**, 171 (1981).
- ¹³P. J. Saathoff and W. H. Melbourne, "Effects of free-stream turbulence on surface pressure fluctuations in a separation bubble," *J. Fluid Mech.* **337**, 1 (1997).
- ¹⁴A. J. Smits, "Scaling parameters for a time-averaged separation bubble," *AIAA J.* **104**, 178 (1982).
- ¹⁵A. Naguib, S. P. Gravante, and C. E. Wark, "Extraction of turbulent wall-pressure time-series using an optimal filtering scheme," *Exp. Fluids* **22**, 14 (1986).
- ¹⁶A. Roshko and J. C. Lau, "Some observations on transition and reattachment of a free shear layer in incompressible flow," *Proceedings of 1965 Heat Transfer and Fluid Mech. Inst.*, 1965.
- ¹⁷I. Lee and H. J. Sung, "Characteristics of wall pressure fluctuations in separated and reattaching flows over a backward-facing step: Part II. Unsteady wavelet analysis," *Exp. Fluids* **30**, 273 (2001).
- ¹⁸P. Huerre and P. A. Monkewitz, "Local and global instabilities in spatially developing flows," *Annu. Rev. Fluid Mech.* **22**, 473 (1990).
- ¹⁹D. Wee, S. Park, T. Yi, A. M. Annaswamy, and A. F. Ghoniem, "Reduced order modeling of reacting shear flow," *AIAA 40th Aerospace Sciences Meeting & Exhibit, AIAA Paper 2002-0478*, January 14–17, Reno, NV, 2002.
- ²⁰A. F. Heenan and J. F. Morrison, "Passive control of backstep flow," *Exp. Therm. Fluid Sci.* **16**, 122 (1998).
- ²¹D. G. Mabey, "Analysis and correlation of data on pressure fluctuations in separated flow," *J. Aircr.* **9**, 642 (1972).
- ²²L. W. Sigurdson, "The structure and control of a turbulent reattaching flow," *J. Fluid Mech.* **298**, 139 (1995).
- ²³M. Kiya, M. Shimizu, and O. Mochizuki, "Sinusoidal forcing of a turbulent separation bubble," *J. Fluid Mech.* **342**, 119 (1997).